Semiconductor optical amplifier based nonlinear optical loop mirror with feedback

W. M. Wong & K. J. Blow
Photonics Research Group, School of Engineering & Applied Science (SEAS), Aston University, Aston Triangle, Birmingham B4 7ET, United Kingdom
tel. +44 121 359 3611, e-mail. w.m.wong@aston.ac.uk

ABSTRACT

The behavior of a semiconductor optical amplifier (SOA)-based nonlinear loop mirror with feedback has been investigated as a potential device for all-optical signal processing. In the feedback device, input signal pulses ('ones') are injected into the loop, and amplified reflected pulses are fed back into the loop as switching pulses. The feedback device has two stable modes of operation – *block mode*, where alternating blocks of 'ones' and 'zeros' are observed, and spontaneous *clock division* mode, where halving of the input repetition rate is achieved. Improved models of the feedback device have been developed to study its performance in different operating conditions. The feedback device could be optimized to give a choice of either of the two stable modes by shifting the arrival time of the switching pulses at the SOA. Theoretically, it was found possible to operate the device at only tens of fJ switching pulse energies if the SOA is biased to produce very high gain in the presence of internal loss. The clock division regime arises from the combination of incomplete SOA gain recovery and memory of the startup sequence that is provided by the feedback. Clock division requires a sufficiently high differential phase shift per unit differential gain, which is related to the SOA linewidth enhancement factor.

Keywords: Nonlinear optical loop mirror; semiconductor optical amplifier; optical switching

1. INTRODUCTION

Substantial work has been reported in semiconductor optical amplifier (SOA) based fiber loop mirrors for all-optical processing such as de-multiplexing [1], logic functions [2, 3], and regenerative memory [4, 5]. The strong nonlinearity of the SOA compared to silica fiber allows shorter loops, thereby improving stability and minimizing latency, thus enabling all-optical bit-serial processing. By providing the loop mirror with feedback, two modes of operation have been reported, both theoretically [6] and experimentally [7]. So far, the performance characteristics of the feedback device have not been extensively investigated. The previous simple model [6] neglected some important effects that may influence the stable modes of behavior of the feedback device, which is extremely sensitive to the phase dynamics at startup. In this work, improved dynamical models of the SOA-based fiber loop mirror with feedback have been developed for better prediction of its behavior. Using the new models, some important effects were identified and the performance characteristics of the feedback device were investigated. The models showed that the feedback device could be optimized to give two stable modes of behavior, and either one could be selected by temporally shifting the fixed-width switching window.

2. BASIC DESCRIPTION OF THE FEEDBACK LOOP MIRROR

The schematic diagram of the SOA-based fiber loop mirror with feedback is given in Fig. 1. The SOA is placed at an offset distance from the mid-point of the fiber loop mirror in order to break the symmetry. This results in a time delay between the counter-propagating signal pulses arriving at the SOA. This configuration is known as either the TOAD [8] or SLALOM [9]. A switching pulse saturates the SOA so that the two counter-propagating (clockwise – cw and counter clockwise – ccw) signal pulses acquire different phase shifts due to the different arrival time at the SOA. The signal pulses recombine at the 50:50 coupler later, and depending on the differential phase shift between the two signal pulses, the recombined pulse is either transmitted or reflected. In the feedback TOAD configuration [6], the reflected signal pulses are amplified and polarization rotated before being fed back into the fiber loop as switching pulses. The only input required for the feedback device is a continuous train of pulses ('ones'). The feedback path contains a maximum of M_{fb} pulses. The two stable modes of operation of the feedback TOAD are described in the following:

WDM and Photonic Switching Devices for Network Applications III, Ray T. Chen, Joseph C. Chon, Editors, Proceedings of SPIE Vol. 4653 (2002) © 2002 SPIE · 0277-786X/02/$15.00

(A) *Block mode* – Initially, the absence of switching pulses from the empty feedback path causes the incoming signal pulses to be reflected. The reflected pulses are selected by the circulator into the feedback path, amplified by the erbium-doped fiber amplifier (EDFA), and are coupled back into the fiber loop as orthogonally-polarized switching pulses. Now, the switching pulses cause the signal pulses to be switched to the transmission port and the feedback path starts to empty. After the last switching pulse is emptied out from the feedback path, the output now switches back to the reflection port. This process repeats itself and the transmitted output contains alternating blocks of M_{fb} pulses ('ones') followed by blocks of 'zeros'. At low repetition rates, it is easy to achieve almost zero differential phase shift ($\Delta\phi \sim 0$) because of full carrier recovery, and this produces near-zero transmission (blocks of 'zeros'). This will give a good contrast ratio but it is ultimately limited by differential gain modulation, which causes partially reflected pulses during blocks of 'ones'. At high repetition rates, full switching to the reflection port becomes more difficult to achieve due to incomplete carrier recovery, and the contrast ratio is further degraded. In block mode, the feedback TOAD acts as an inverting circulating shift register [10].

(B) *Clock division mode* – At high repetition rates the SOA gain could not recover fast enough to its equilibrium level before the next switching pulse arrives. Hence, pulse-to-pulse interactions occur that leads to complex dynamical behavior. The startup sequence is crucial in predicting the stable mode of operation, as the group of M_{fb} reflected pulses are stored in memory by the feedback loop, and affects the carrier dynamics in the next circulation. If an initial pulse amplitude modulation is enhanced on each circulation, it propagates through the block of M_{fb} pulses and grows in magnitude until every second pulse in the block is either switched or not. This is the stable clock division mode. The maximum number of pulses contained in the feedback path (M_{fb}) should be an *odd* integer for complete spontaneous clock division to occur. If silica fiber were used, then clock division would not have been possible because the lifetime of the nonlinear response of silica is ultra-fast (fs). Clock division is useful in demultiplexing since a clock rate at a sub-multiple of the line rate is required, while clock recovery schemes usually give the original line rate.

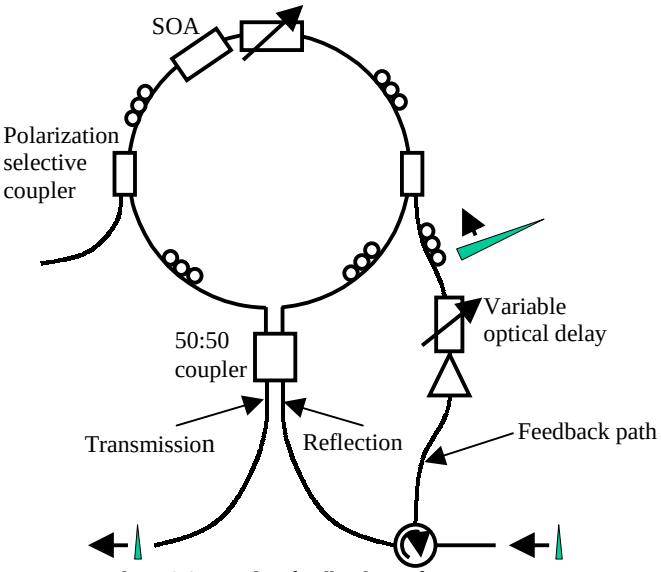

Fig. 1 The TOAD with a feedback configuration.

3. MODELING THE DEVICE

Previously, a simple model of the feedback TOAD was developed based on recursive carrier recovery equations. In the model, ideal Dirac delta pulses were assumed, while differential gain modulation and inhomogeneous effects in the SOA were not considered [6]. In this work, a traveling-wave (TW) version of the feedback TOAD model has been developed taking into account:

(i) pulse shape
(ii) gain saturation along the SOA
(iii) differential gain modulation between counter propagating signal pulses

(iv) SOA internal loss (α_{int})
(v) carrier dependence of the SOA recovery lifetime.

The TW model was used to identify the role of each of these effects in predicting the feedback TOAD behavior. In the TW model, the SOA was divided into several smaller but equal-length sections to include inhomogeneous effects. The pulse evolution and carrier dynamics are solved at each unit section as the switching pulse travels across the SOA. One main assumption in the TW model is that only the higher energy switching pulses, not the signal pulses, saturate the SOA. The relative positions in time between the cw, ccw, and switching pulses in the fiber loop must be known during the passage of the signal pulses across the SOA. It is worth pointing out that the traveling-wave equations for the cw pulse are solved in the opposite direction to the ccw pulse. Since the signal pulses undergo almost equal total phase shifts outside the SOA and the fiber loop is short, only the phase shifts caused by the nonlinear SOA are considered. It was also assumed that losses are not present in the fiber loop, 50:50 coupler, and other components in the feedback loop mirror since these do not affect the switching properties of the device. In the models, the switching pulses are simply the signal pulses amplified by the SOA.

Simulations showed that adequate accuracy could only be achieved if we use 10 sections or above in the TW model. If fewer than 10 sections were used in the model, clock division behavior could not be observed because the differential phase shift was underestimated while the differential gain was overestimated. Clock division requires a substantial amount of differential phase shift per unit differential gain. This relationship between phase and gain change is governed by the linewidth enhancement factor, α_H. Unfortunately, the 10-section TW model takes a long time to run, and optimization of device performance is impractical. To achieve faster simulation speed, the integrated carrier traveling-wave model (ICTW) model has been developed. By using the ICTW model, faster convergence is possible and only 3 sections are required to give the same results obtained from a 10-section TW model. However, the simulation time taken is still impractical for a performance study of the feedback device. This is especially true for low repetition rates (f) and a long feedback path (M_{fb}), in which a very large number of pulses must be simulated before the stable mode of behavior is reached. Therefore, the previous simple model was refined by including the traveling-wave effects in a heuristic approach. A constant effective lifetime was used in the simple model since it was found to be accurate to within ±10% of the carrier dependent lifetime even for large variations in amplified pulse energies (7fJ to 333pJ). The refined simple model is much more computationally efficient than its traveling-wave counterpart yet simulation results from both models agree favorably. Therefore, the more efficient simple model has been used to investigate the behavior and performance of the feedback TOAD. A detailed description of the models will be discussed elsewhere. The parameters used in the models are listed in Table 1.

Table 1. Fixed parameters used in the models.

PARAMETERS	**VALUES**
Length, L	1000μm
Width, w	1μm
Thickness, d	0.2μm
Wavelength, λ	1.55μm
Confinement factor, Γ	0.3
Differential gain constant, g	$4.2 \times 10^{-20}\text{m}^2$
Internal loss, α_{int}	30cm^{-1}
Transparency carrier density, N_0	$1 \times 10^{24}\text{m}^{-3}$
Effective group index, n_g	4
FWHM of input signal pulses	2ps
Index change per unit inversion, n_{eh}	$4 \times 10^{-26}\text{m}^3$
Linewidth enhancement factor, α_H	7.7
Nonradiative recombination constant, A_{nr}	$2 \times 10^{8}\text{s}^{-1}$
Bimolecular recombination constant, B_{rad}	$40 \times 10^{-16}\text{m}^3\text{s}^{-1}$
Auger recombination constant, C_{aug}	$10 \times 10^{-41}\text{m}^6\text{s}^{-1}$
Effective carrier recovery lifetime, τ_{eff}	80ps

4. RESULTS AND DISCUSSION

For a given set of device parameters, the feedback TOAD behavior is directly controllable by adjusting the following:

(i) relative position in time of switching window (T_1:T_2)
(ii) switching window width ($2\Delta T$)
(iii) bias level of the SOA (I_b)
(iv) signal pulse energy (E_{in})
(v) repetition rate of signal pulses (f)

The switching window position could be shifted in time by controlling the arrival time of the switching pulse at the SOA relative to the signal pulses. The relative position of the switching window is denoted as T_1:T_2, where T_1(T_2) is the time delay between the arrival of the clockwise (counter clockwise) and switching pulses at the SOA. The offset distance from the fiber loop center gives the window width. Controlling the bias current gives different amounts of maximum available phase shift, ϕ_{max} and unsaturated gain, G_0. For a given stable mode of operation, the adjustable parameters (i)-(v) are related to one another.

1. Two selectable stable modes of operation – block mode and clock division

It has been reported experimentally that by shifting the arrival time of the switching pulse relative to the signal pulses, either of the two modes of operation could be selected but higher pulse energy was required to achieve the block mode [7]. Using the refined simple model, the feedback TOAD has been optimized to give two selectable modes of operation for a fixed window width of 80ps (see Fig. 2). The same behavior could also be achieved using the TW model. All simulations were done with the feedback TOAD operating at 5GHz unless otherwise stated. The relative position of the window (T_1:T_2) was chosen to be 0ps:80ps and 80ps:160ps for the clock division and block modes, respectively. No adjustment of the pulse energy was necessary when the block mode was selected. It is worth pointing out that better contrast ratios can be achieved if one of the two modes of behavior is optimized *separately*. The block mode works better at lower repetition rates while the clock division mode prefers higher repetition rates. The two modes of operation may be extended to higher bit rates by controlling the SOA recovery lifetime using a holding beam [11].

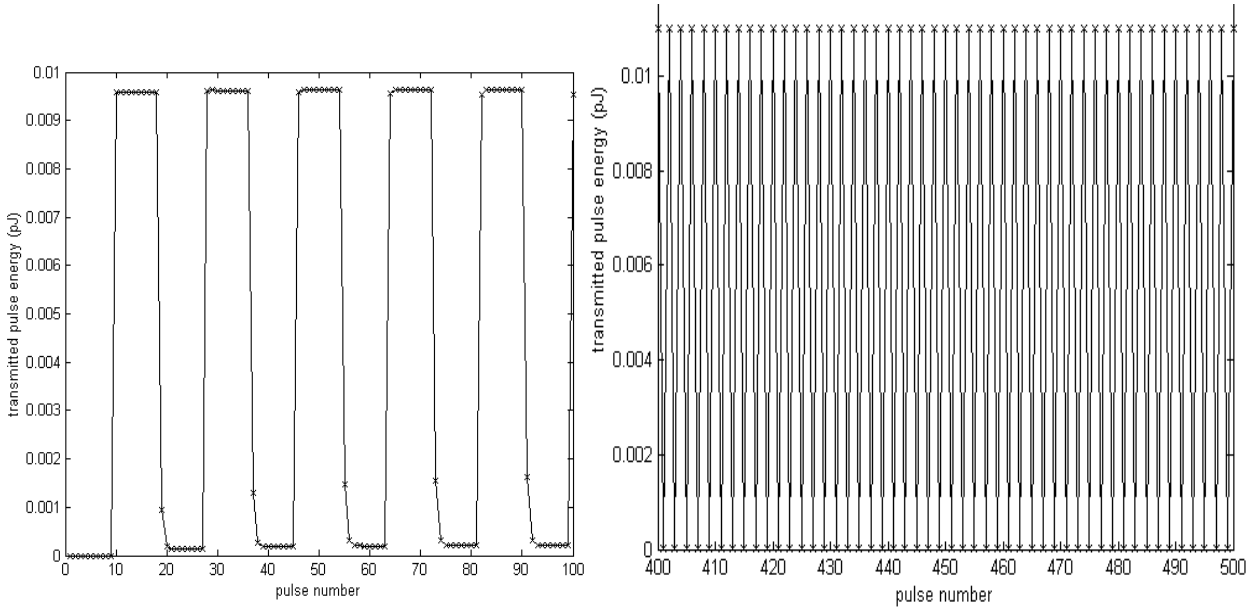

(a) (b)

Fig. 2 Either (a) block mode or (b) clock division could be selected by shifting the arrival time of the switching pulse at the SOA by 80ps. The feedback TOAD is operated at 5GHz and has a feedback path length of M_{fb} = 9.

In Fig. 2(a), one 'renegade' pulse from the block of zeros is clearly observed. This can be explained as follows. Ideally, a zero differential phase shift ($\Delta\phi$) between the counter-propagating signal pulses is necessary to produce the blocks of 'zeros' (100% reflection). Unfortunately, after the feedback path has emptied, the carrier population (phase) continues

to recover as shown in Fig. 3(a), producing a non-zero $\Delta\phi$, causing the first 'zero' pulse to be partially transmitted. The subsequent 'zeros' occupy a lower level but this 'zero' level (hence also the contrast ratio) is limited by differential gain modulation. This is because differential gain modulation causes some fraction of pulse energy to be reflected into the feedback path even if $\Delta\phi=\pi$ is achieved during the blocks of 'ones'. These residual pulses will produce non-zero $\Delta\phi$ in the next circulation and eventually limit the lowest possible 'zero' level. For clock division mode, the optimized contrast ratio is much better, usually above 25dB. Fig. 3(b) shows the initial phase dynamics that lead to clock division, where cross-points between the accumulated phase shifts of cw and ccw pulses could be observed. This means that $\Delta\phi$ = 0 (100% reflection) and $E_{cw} = E_{ccw}$ (no differential pulse amplitude), giving almost perfect 'zeros' in the transmitted output. The large phase shifts in Fig. 3 are due to the high SOA bias level that corresponds to G_0 = 25dB.

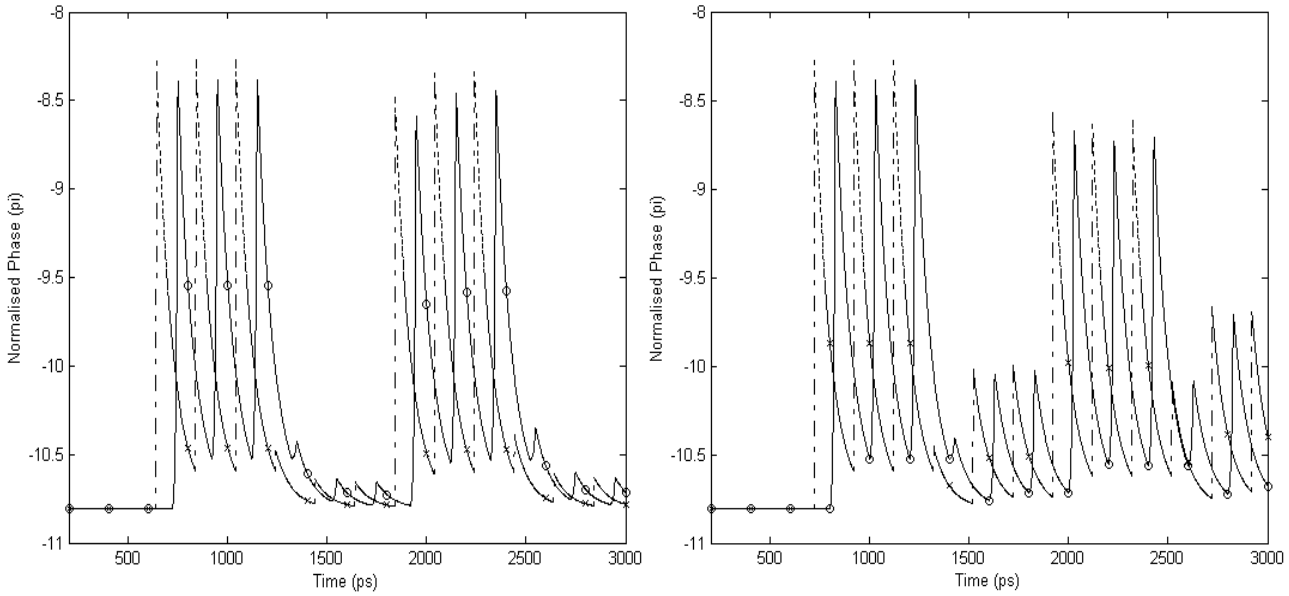

(a) (b)

Fig. 3 Initial phase dynamics for cw (solid -) and ccw (dash-dot -.-) signal pulses that give (a) block mode (b) clock division mode for M_{fb} = 3. The circles (o) and crosses (x) mark the phase shift seen by the cw and ccw signal pulses when they recombine at the 50:50 coupler after traversing the fiber loop.

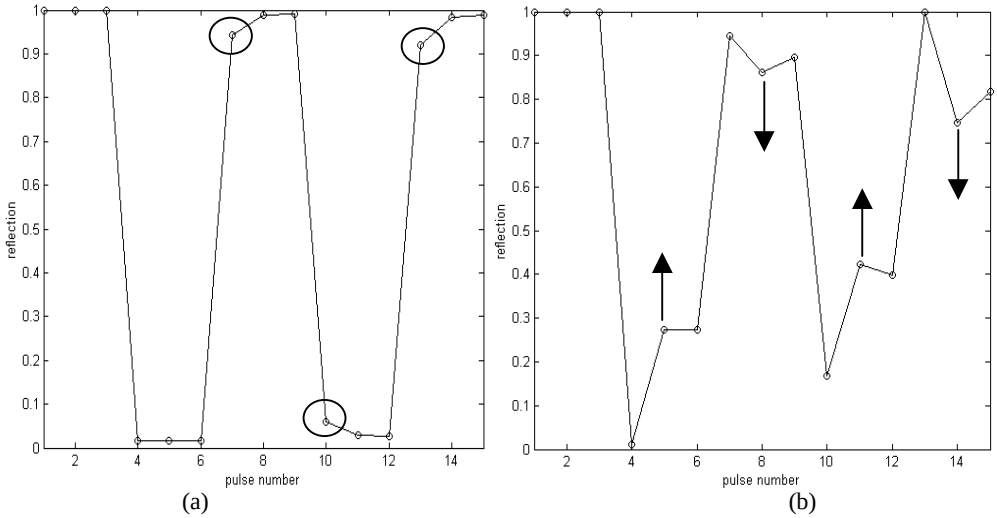

(a) (b)

Fig. 4 The startup sequences for (a) block mode (b) clock division. The circles show the imperfect switching due to incomplete carrier recovery during block mode operation. The arrows show the amplitude modulation growing with the number of circulations eventually leading to clock division.

Two different startup sequences for the block mode and clock division are shown in Fig. 4(a) and (b), respectively. The reflected pulse energy is plotted against its corresponding pulse number for a device with a feedback path length of M_{fb} = 3. The differential gain modulation effect is not included here to clearly show the startup sequence due only to phase dynamics. In the reflection response, almost 100% reflection is possible when $\Delta\phi = 0$ because there is almost zero differential pulse amplitude.

2. SOA bias level

The bias level of the SOA defines the equilibrium carrier density level (N_{ss}), which gives the maximum phase shift (ϕ_{max}), while the switching pulse energy defines the maximum phase change ($\Delta\phi_{max}$). For block mode, $\Delta\phi_{max}$ at startup is ~ π while for clock division $\Delta\phi_{max}$ at startup is between 0.5π and π. For a given bias level, ϕ_{max} may be equal to several π but the switching pulse energy is only required to produce $\Delta\phi_{max}$ of ($\pi \pm 0.5\pi$). The input and first feedback pulse energies required for operating the feedback TOAD are plotted against the SOA unsaturated gains in Fig. 5(a) and (b), respectively, with SOA internal loss (α_{int}) as parameter. The values of unsaturated gain correspond to SOA bias levels from 510mA to 550mA for α_{int} = 0cm^{-1} (580mA to 650mA for α_{int} = 30cm^{-1}) in steps of 10mA, as shown in Table 2. The results show that the feedback device with higher SOA gain can be operated at smaller input pulse energy. The pulse energies are optimized to obtain a contrast ratio of ~ 40dB in clock division mode. In block mode, one pulse in each block usually experiences imperfect switching. The worst-case contrast ratio is taken by using the lowest-energy 'one' and highest-energy 'zero'. In all cases, the minimum contrast ratio is ~ 7dB but the maximum contrast ratio can be higher than 15dB. The maximum contrast ratio was previously found to be limited to ~15dB by differential gain modulation for a pulse amplitude difference of 3dB [7].

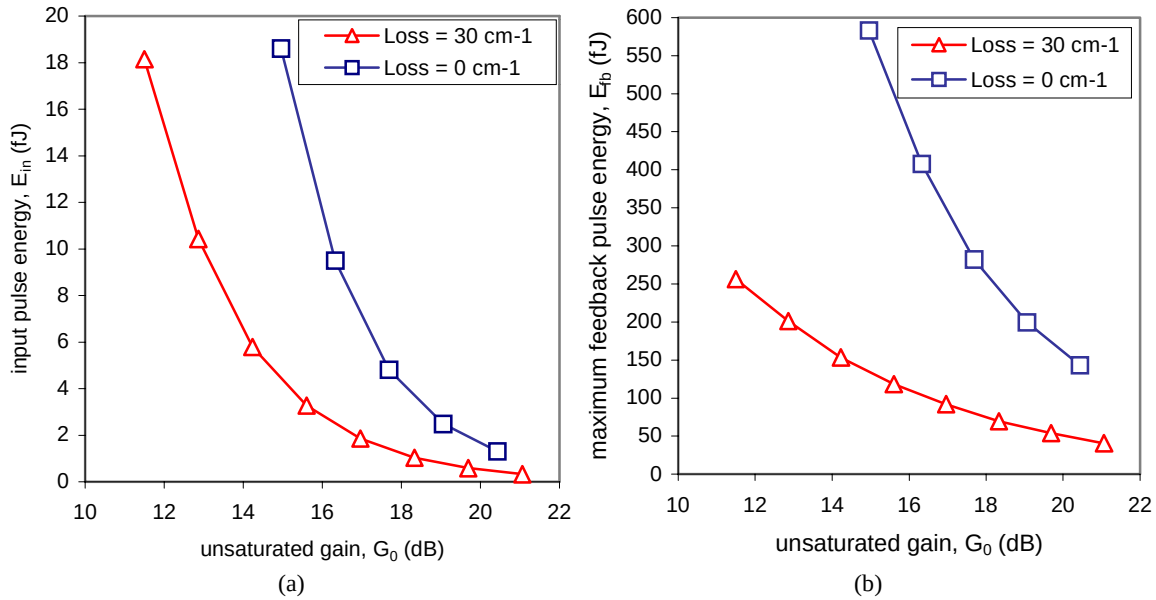

(a) (b)

Fig. 5 (a) Input pulse energy and (b) first feedback pulse energy against unsaturated gain.

At high SOA gain, the pulse energies were lower than experimentally observed because losses were not considered throughout the fiber loop and its components except in the SOA. In the presence of significant SOA internal loss, much higher carrier densities are needed to obtain the same amount of *net* gain, hence the operating pulse energies are smaller than in the lossless case. The results were restricted to input pulse energies below 20fJ so that they would not contribute to the carrier dynamics, which is an important assumption of the model. The range of switching pulse energies was below 600fJ (E_{sat} ~ 2pJ), which means that the feedback TOAD is mainly operating in the unsaturated regime. The fact that the SOA bias current levels were higher than those used in experiment is purely an artifact resulting from the constant effective lifetime used in the simple model, which was chosen to match the dynamical lifetime. The TW model with a carrier dependent lifetime would give more realistic SOA bias levels in agreement with experimental results [7].

Table 2 Feedback pulse energies to achieve contrast ratio of 40dB in clock division mode for (a) $\alpha_{int} = 0cm^{-1}$ (b) $\alpha_{int} = 30cm^{-1}$

(a) Bias level (Unsaturated Gain)	Input pulse energy, E_{in} (fJ)	First feedback pulse energy, E_{fb} (fJ)	Contrast Ratio (dB) Clk Div / Blk Mod
510mA (14.96dB)	18.57	582.01	40.37 (7.24)
520mA (16.33dB)	9.330	400.53	40.22 (7.20)
530mA (17.69dB)	4.780	281.07	40.49 (7.18)
540mA (19.06dB)	2.477	199.50	40.02 (7.15)
550mA (20.43dB)	1.320	145.62	40.41 (7.35)
(b) Bias level (Unsaturated Gain)	Input pulse energy, E_{in} (fJ)	First feedback pulse energy, E_{fb} (fJ)	Contrast Ratio (dB) Clk Div / Blk Mod
580mA (11.50dB)	18.150	256.18	40.76 (6.76)
590mA (12.86dB)	10.420	201.45	40.79 (7.17)
600mA (14.23dB)	5.790	153.32	40.51 (6.82)
610mA (15.60dB)	3.257	118.13	40.70 (6.86)
620mA (16.96dB)	1.855	92.16	40.30 (7.25)
630mA (18.33dB)	1.021	69.48	40.36 (6.91)
640mA (19.69dB)	0.5695	53.08	40.82 (6.94)
650mA (21.06dB)	0.3167	40.43	40.90 (6.97)

3. TOAD switching window width

The influence of the switching window width on the performance of the feedback TOAD was next investigated. For clock division mode, the input signal pulse energies (E_{in}) were adjusted to give contrast ratios nearest to 15dB as higher contrast ratios may be difficult for very small/large windows. The results are plotted in Fig. 6. For all TOAD window widths, the cw signal pulse is adjusted so that it exits the SOA at exactly the same time as the switching pulse arrives (t = 0ps). The cw pulse has therefore not experienced the gain saturation caused by the switching pulse. The ccw signal pulse arrives at the SOA $2\Delta T$ later, where ΔT is the propagation delay time that corresponds to the offset distance away from the mid-point of the fiber loop. The relative position of the TOAD window (T_1:T_2) is therefore denoted as 0ps: $x$ps, where x is a variable. Fig. 6(a) shows that higher switching energies are required for wider windows. This is because for the same switching pulse energy, a wider TOAD window means that more carrier recovery would have occurred when the ccw pulse arrives at the SOA, hence producing a smaller $\Delta\phi$.

For an 80ps window, the number of circulations to reach clock division as a function of feedback path length (M_{fb}) is plotted in Fig. 6(b). It increases almost linearly with the feedback path length. Fig. 7(a) shows the number of circulations it takes to reach clock division as the TOAD window width is varied from 20ps to 80ps (10% to 40% of the repetition period of 200ps). To save simulation time, the feedback path was assumed to be short, that is M_{fb} = 3. The simulation results show that narrow windows are not desirable as they lead to very slow clock division, especially when the feedback path is long. In a practical setup, it is difficult to obtain a feedback loop that consists of less than thousands of pulses. Simulations show that for a 20ps window ($\alpha_{int} = 30cm^{-1}$), even for a feedback length of only 15 pulses, complete clock division took around 4500 circulations.

For block mode operation, the TOAD window width is again varied from 20ps to 80ps but the switching pulse is set to arrive exactly in between the cw and ccw pulses for all cases. Previously, it was believed that block mode could only be achieved by setting the switching pulse to arrive at the SOA before both the cw and ccw signal pulses [7]. However, the model shows that block mode is possible even if the switching pulse arrives in between the cw and ccw pulses. Fig. 7 (a) and (b) show that narrow windows lead to slow clock division while wider windows need only slightly more circulations to reach stable block mode.

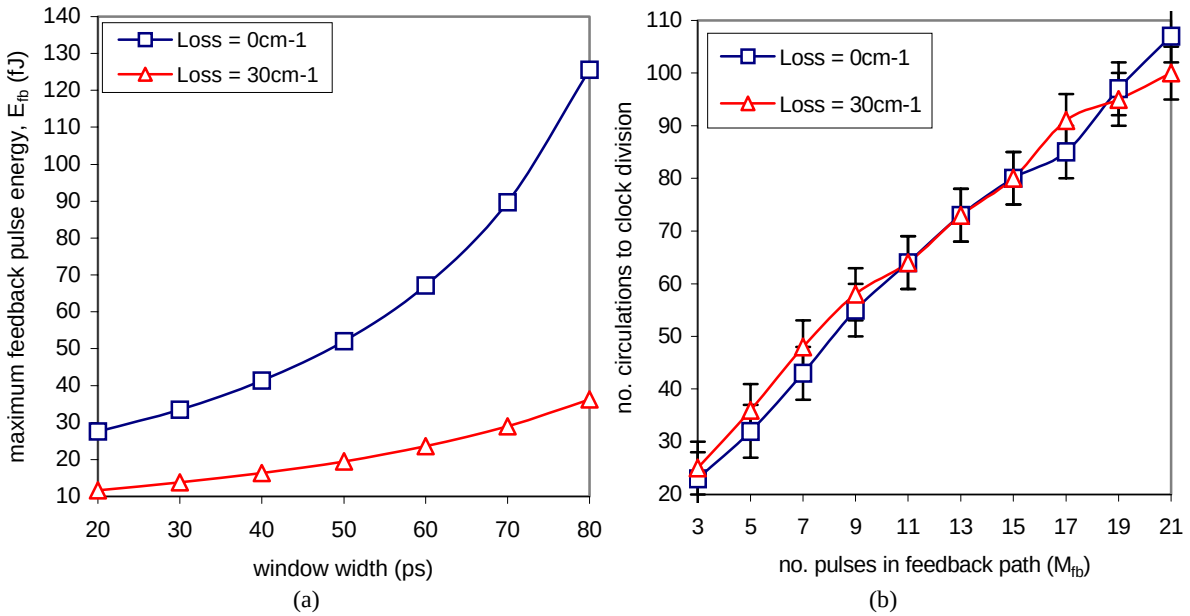

Fig. 6 (a) The first feedback pulse energy required to achieve pure clock division with contrast ratio of 15dB as a function TOAD window width (b) The dependence of number of circulations to reach clock division on the feedback path length (M_{fb}) for a 80ps window. The error bars are included due to the ambiguity of taking the exact pulse number at which clock division is complete.

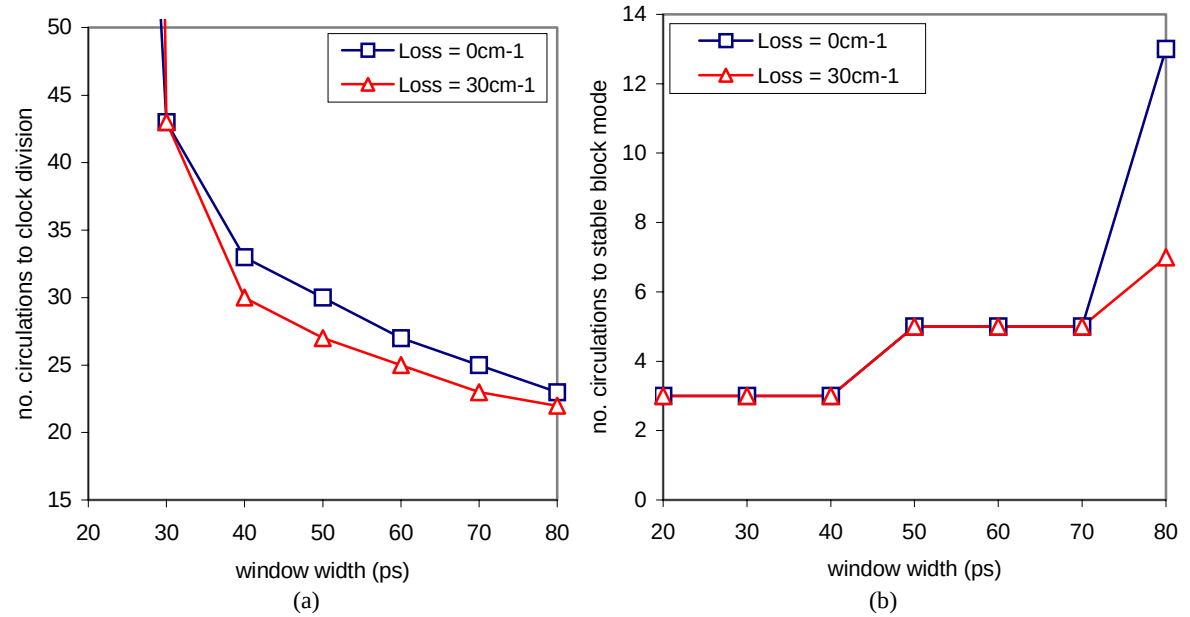

Fig. 7 The influence of switching window width on total number of circulations to achieve (a) clock division (b) stable block mode.

Fig. 8 (a) and (b) show the contrast ratios for clock division and block mode, respectively. The pulse energies were chosen to give contrast ratios very close to 15dB for clock division as explained earlier. For each window width, the block mode could be selected by adjusting the switching pulse to arrive exactly in between the cw and ccw signal pulses. The contrast ratios for the block mode deviates from 15dB for wider windows but are within ±5dB. The contrast ratios are plotted for the worst case using the lowest-energy 'one' and highest-energy 'zero'. Therefore, reasonably good contrast ratios (~15dB) could be obtained for all window widths from 20ps to 80ps in both modes of operation.

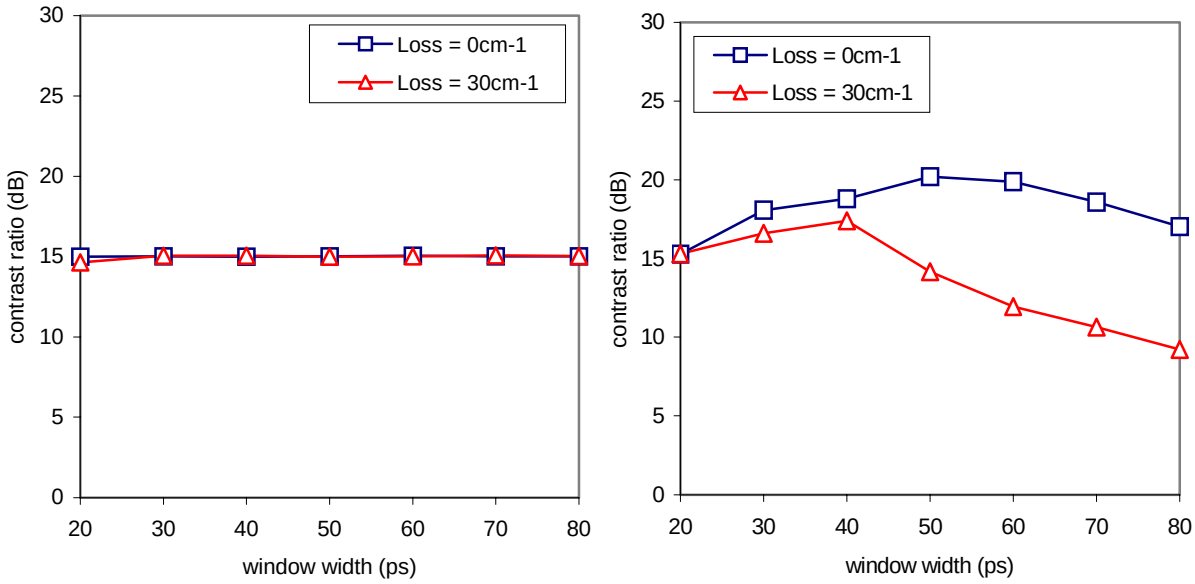

Fig. 8 The contrast ratio against TOAD window width for (a) clock division (b) block mode. The pulse energies used for each TOAD window width correspond to the values plotted in Fig. 6(a).

4. Signal repetition rate

The performance of the feedback device as a function of the signal repetition rate (f) was also studied for both modes of operation. The TOAD window was chosen to cover 40% of the repetition period ($T = 1/f$) in all cases but its relative position in time could be shifted to select either block mode or clock division.

Clock division mode: The feedback TOAD was optimized, by varying the input pulse energies, to give the best contrast ratios during complete clock division for different signal repetition rates. The results are plotted in Fig. 9. Simulations showed that fluctuations exist in the optimized contrast ratios, which is believed to be due to the sensitivity of the device behavior to its phase dynamics. However, the maximum contrast ratios are above 25dB for all cases. The repetition period is divided into 100 smaller time steps in each case. The relative time position of the TOAD window is denoted as T'_1:T'_2 = 0:40 for clock division mode. T'_1:T'_2 does not give a fixed window width but is repetition rate dependent. For example, a 5GHz signal would have the cw pulse exiting the SOA at the same time ($T_1 = 0 \times T/100$) as the switching pulse arrives, while the ccw pulse exits the SOA at 80ps later ($T_2 = 40 \times T/100$).

To achieve clock division, the product of effective recovery lifetime and signal repetition rate should lie between 0.24 and 1.36 when internal loss is significant ($\alpha_{int} = 30cm^{-1}$), while it should be between 0.32 to 1.20 in the lossless case ($\alpha_{int} = 0cm^{-1}$). The limits are taken from the lowest/highest repetition rates just before the switching pulse energies sharply rise above 500fJ. The range of the lifetime-repetition rate product is wider than was previously reported (from 0.6 to 1.2) [12]. For a given recovery lifetime, the inclusion of differential gain modulation in the new model was expected to narrow down the range of repetition rates that allow clock division. However, the constant n_{eh}, which governs the amount of cross-phase modulation, was taken to be twice the value used previously. This corresponds to a linewidth enhancement factor of ~ 8, which agrees better with the measured value of 9 in the experiments [7]. Therefore, clock division could be achieved for signal repetition rates extending over a range of > 10GHz.

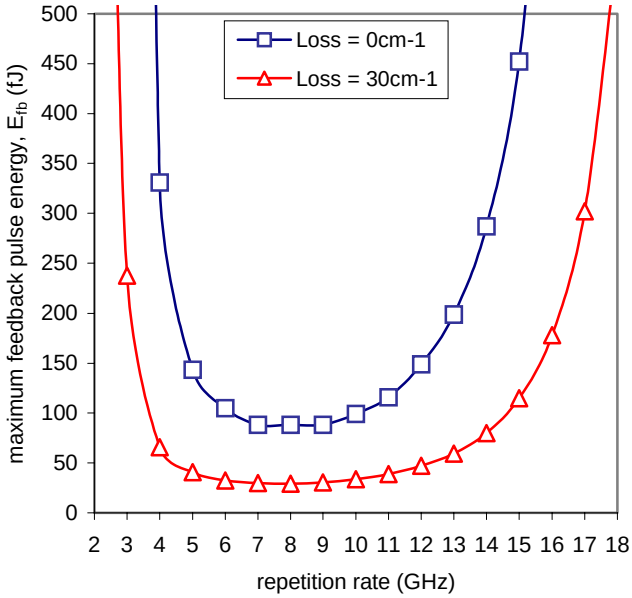

Fig. 9 Clock division: The switching pulse energy for maximum contrast ratio as signal repetition rate is varied.

Clock division is difficult at low repetition rates (<4GHz) because there is only little pulse-to-pulse interaction and the carrier density almost recovers to its equilibrium level. In contrast, at high repetition rates (>15GHz), the pulse-to-pulse interaction is strong leaving little time for the carrier density to recover. In both cases, the differential phase shifts are too small to initiate clock division mode. Therefore, high switching pulse energies are required to force the system into clock division at these non-optimal (very low/high) signal repetition rates. Clock division ceases at repetition rates well below 3.5GHz and above 18GHz for the case with significant SOA internal loss. The phase dynamics at these limits are plotted in Fig. 10 (a) and (b), which shows (a) large phase shift fluctuations but small pulse-to-pulse interactions and (b) small phase shift fluctuations but large pulse-to-pulse interactions, respectively.

Block mode: The performance of block mode (T'_1:T'_2 = 40:80) at different signal repetition rates was also investigated. In Fig. 11(a), it is clear that the contrast ratio drops rapidly as the repetition rate is further away from its optimum value. The (worst-case) contrast ratios for the block mode are significantly lower (by >10dB) than for clock division. The contrast ratio drops rapidly at lower repetition rates (<3GHz) because the carrier has almost recovered to its equilibrium level after 40% of the repetition period, which results in differential phase shifts ($\Delta\phi$) too small for block mode operation. When internal loss is present (α_{int} = 30cm^{-1}), the lifetime-repetition rate product is between 0.20 and 0.44, while it is between 0.24 to 0.40 in the lossless case (α_{int} = 0cm^{-1}). The limits are taken from the repetition rates at which contrast ratios start to fall below 8dB. The range of repetition rates for block mode operation is much smaller than for clock division in this window position. The pulse energies that are optimized for maximum contrast ratios are shown in Fig. 11(b). At low repetition rates, high pulse energies are needed so that the signal pulses acquire enough differential phase shifts after a delay time of 40% of the repetition period.

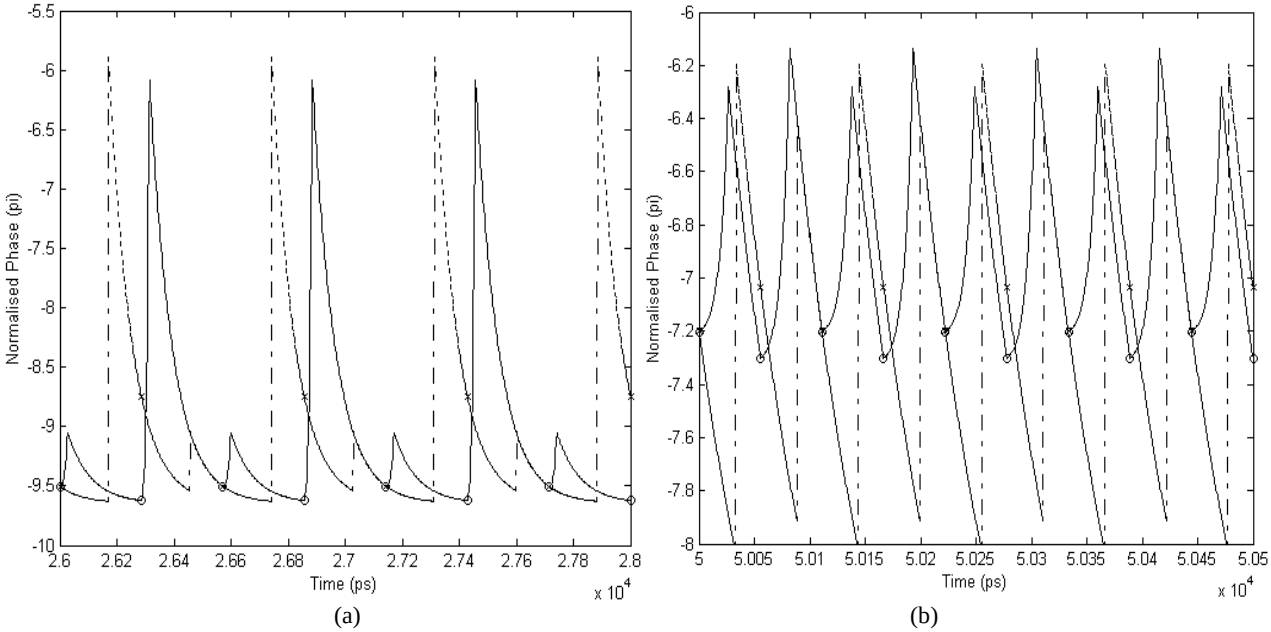

Fig. 10 Phase dynamics of cw pulse (solid -) and ccw pulse (dash-dotted -.-) during complete clock division for signal repetition rates of (a) 3.5GHz (b) 18GHz. The circles (o) and crosses (×) mark the accumulated phase shifts seen by the cw and ccw signal pulses, respectively (α_{int} = 30cm^{-1}).

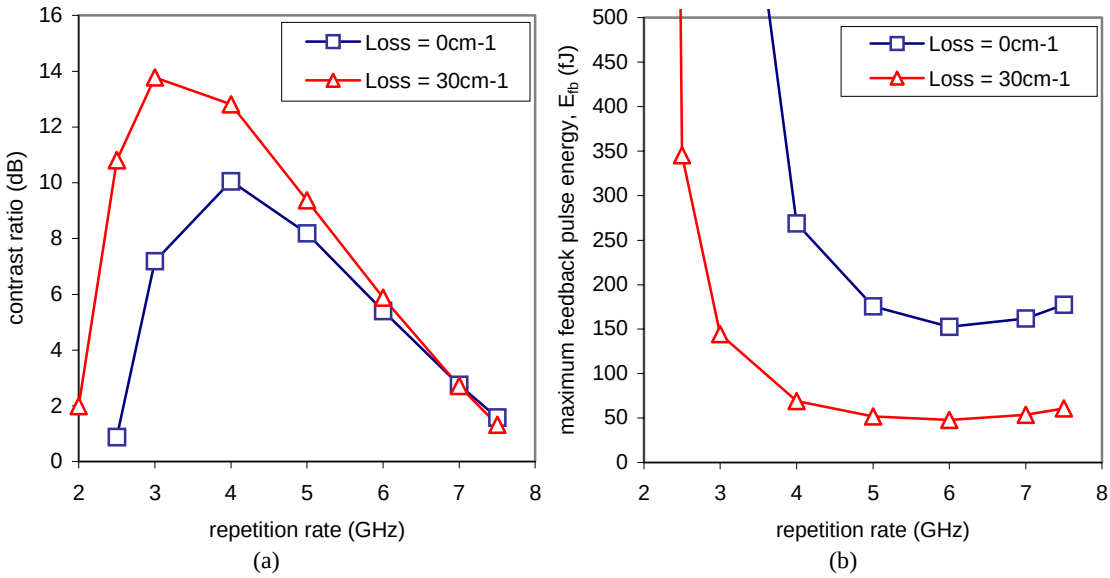

Fig. 11 Block mode operation: Dependence of (a) maximum contrast ratio and (b) switching pulse energy on repetition rate for TOAD window position of T'_1:T'_2 = 40:80.

At low repetition rates, the switching window should cover the early part of the phase dynamics, where most of the recovery occurs, so that we can get a π-phase change to initiate block mode operation. Simulations confirmed that better contrast ratios could be achieved during block mode operation if we use T'_1:T'_2 = 20:60, as shown in Fig. 12(a). Even for signal repetition rates as low as 2GHz, contrast ratios above 15dB could be achieved. This is because the counter-propagating pulses acquire higher differential phase shifts after a time delay of only 20% of the repetition period compared to 40% previously. Ultimately, the contrast ratio in block mode operation is limited by the imperfect transmission (<100%) due to differential gain modulation. The required switching pulse energies are also lower for this new window position as shown in Fig. 12(b). It is also interesting to note that block mode operation at 5GHz is only

slightly affected by the window position. In Fig. 11(a) and Fig. 12(a), the contrast ratios at 5GHz stay around 8-9dB regardless of the window position.

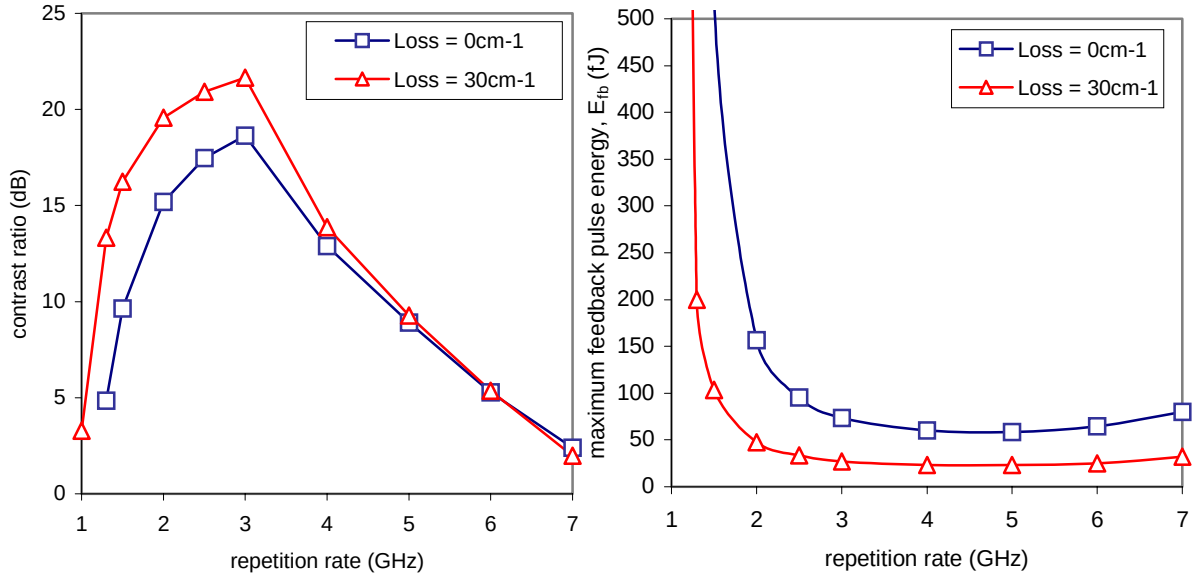

Fig. 12 Block mode operation: Dependence of (a) maximum contrast ratio and (b) switching pulse energy on repetition rate for $T'_1:T'_2$ = 20:60.

5. Pulse energy

Once the stable mode of operation is established, it is worth finding out how the device performance is affected by changes in the pulse energy. Fig. 13(a) shows the contrast ratios for block mode and clock division as the feedback pulse energy is varied for the device with significant SOA internal loss (α_{int} = 30cm^{-1}) and feedback path length of M_{fb} = 3. The maximum contrast ratio is ~50dB when the first feedback pulse energy is ~40fJ. The operating range of pulse energies in clock division mode is ~34fJ (>80% of the optimum energy). If the pulse energy is too small, clock division ceases and the output contains a continuous train of 'ones'. At pulse energies larger than the optimum value, clock division might break down if the feedback path length becomes long enough. As an example, perfect clock division could not be achieved at E_{fb} = 53.6fJ if M_{fb} > 51, as indicated in Fig. 13(a). At even higher pulse energies, clock division breaks down at shorter feedback path lengths. The feedback path length does not affect pulse energies below the optimum value. In block mode, the maximum deviation in contrast ratio is only ~ 4dB as the pulse energy is varied. If the pulse energy is too low, the block mode breaks down – the output now consists of pulses with a sinusoidal-like variation in energy and at even lower switching pulse energies, the output finally becomes a continuous train of pulses with equal energy. At very high pulse energies, the period-four motion sets in. The operating range of pulse energies for block mode is ~ 45fJ (>85 % of the optimum energy). The block mode behavior is insensitive to the feedback path length.

The sensitivity of both modes of operation to pulse energy change in the device with a lossless SOA (α_{int} = 0cm^{-1}) and feedback path length of M_{fb} = 3 is plotted in Fig. 13(b). In clock division mode, the maximum contrast ratio is ~55dB at feedback pulse energy of ~145fJ. The range of pulse energy allowed for pure clock division is ~200fJ (>135% of the optimum energy). This shows that the feedback device with negligible SOA internal loss is less sensitive to pulse energy change. If the clock division output is not optimized for maximum contrast ratio and the pulse energy falls on the higher energy side, a large number of pulses in the feedback path may cause clock division to fail. The block mode experiences only a small deviation in contrast ratio (<3.5dB) as pulse energy is varied. The operating range of pulse energies for block mode is ~170fJ (>95% of the optimum energy).

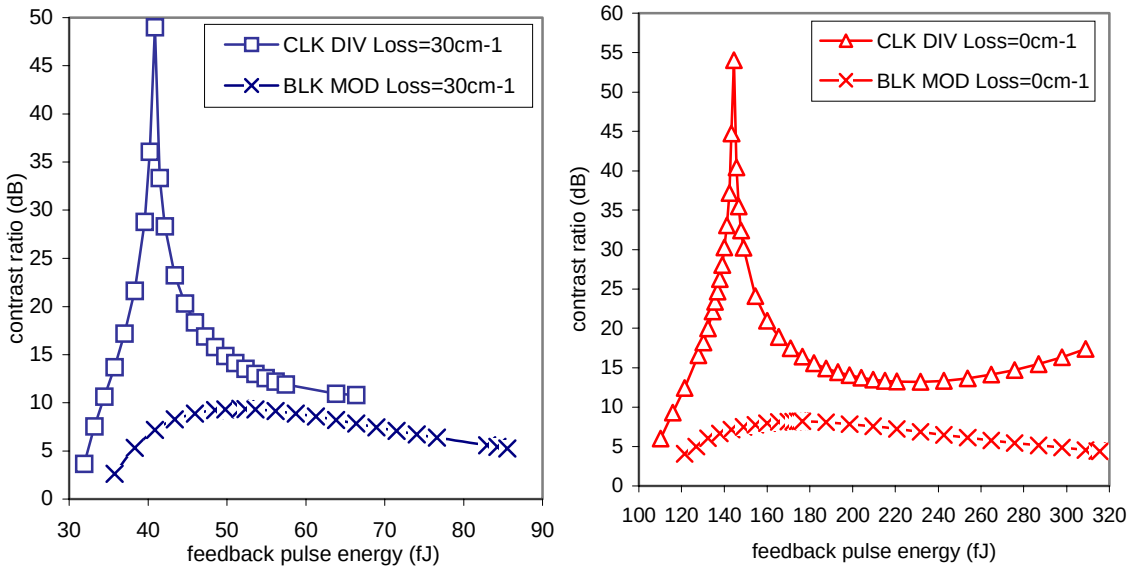

(a) (b)

Fig. 13 Sensitivity of contrast ratios in block mode and clock division to pulse energy change for (a) $\alpha_{int} = 30cm^{-1}$ (b) $\alpha_{int} = 0cm^{-1}$.

6. TOAD switching window shift

The effect of shifting the arrival time of the switching pulses on the performance of the feedback device is plotted in Fig. 14(a) and (b) for block mode and clock division, respectively. In clock division, the pulse energy was chosen to give the maximum contrast ratio for the window position of T_1:T_2 = 0ps:80ps. The switching pulse was then adjusted to arrive later (negative shift) and earlier (positive shift) in time relative to the signal pulses. The maximum total window shift for stable clock division occurs in a device with the shortest feedback path (M_{fb} = 3) and is 20ps. The actual tolerance to the window shift is less than that because pure clock division fails at longer feedback paths. For example, if the window shift is –12ps, clock division breaks down if $M_{fb} > 9$. The tolerance to the window shift is not symmetrical about the original window position – clock division is more stable for a negative shift in time (up to –16ps), while it is more sensitive to the positive shift (only up to +4ps). The tolerance of clock division to the window shift for (i) $\alpha_{int} = 30cm^{-1}$ and (ii) $\alpha_{int} = 0cm^{-1}$ are almost the same. Surprisingly, the reported experimental results were more promising as both modes of operation were stable to within ± 12ps (total shift of 24ps) deviation in switching pulse arrival time in a device running at repetition rates of up to 20GHz. [7].

In block mode operation, greater window shifts are allowed as shown in Fig. 14(b). For $\alpha_{int} = 0cm^{-1}$, the total window shift allowed for stable block mode is 26ps while it is wider for $\alpha_{int} = 30cm^{-1}$, which is 34ps. Similar to the clock division mode, the contrast ratios for the block mode are also not symmetrical about the optimum position of T_1:T_2 = 80ps:160ps. The effect of feedback path length on block mode operation is negligible.

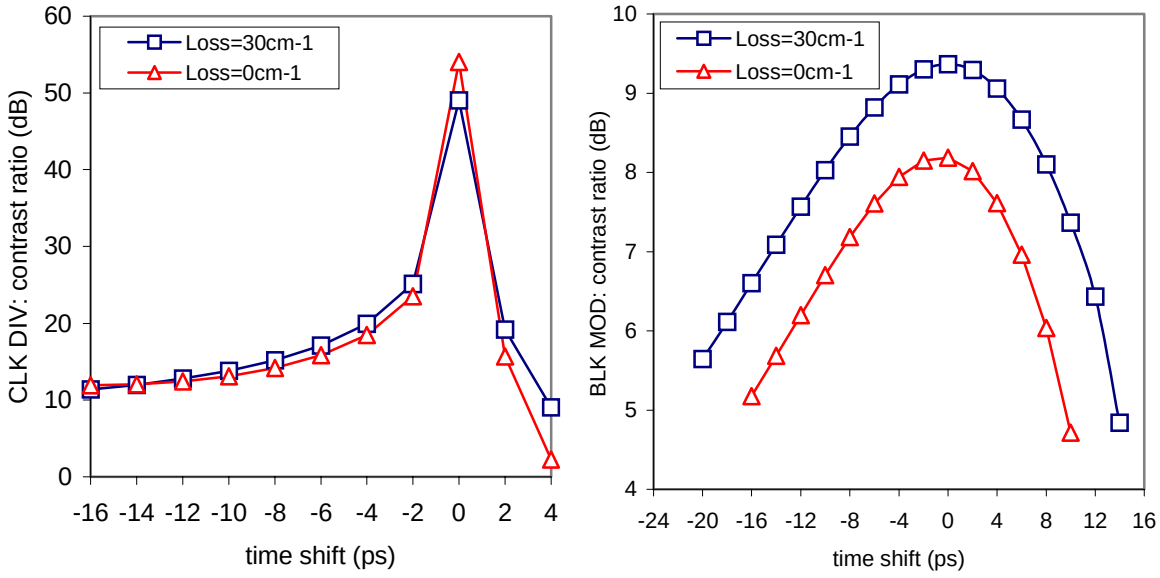

(a) (b)

Fig. 14 Sensitivity of contrast ratio to TOAD window time shift for (a) clock division (b) block mode.

5. CONCLUSION

Several important considerations that affect the phase-sensitive dynamical behavior of the SOA-based fiber loop mirror (TOAD) with feedback have been identified and incorporated into improved models. It was found that carrier dependent SOA lifetimes could be accurately modeled by an effective lifetime without any significant deviation in the device dynamics. This allowed simple carrier recovery equations to be used in the simple model that includes the major dynamical effects of the device. Many of the experimental observations have been modeled but some discrepancies remain, which may be due to some uncertain values of SOA parameters used. It was found that operating pulse energies are significantly affected by the presence of SOA internal loss, which is a quantity worthy of further characterization for accurate modeling of the feedback device. The performance of the feedback device has been investigated based on two selectable stable modes of operation – block mode and clock division. It was shown that good contrast ratios (~15dB) could be obtained for *both* block and clock division modes in the feedback device with an SOA effective lifetime of 80ps. In block mode, the feedback device acts as an inverting circulating shift register while the self-starting clock division mode is useful in demultiplexing, which requires a clock rate that is a sub-multiple of the line rate. By cascading n of these feedback devices, the clock division mode can be extended to divide–by–2^n operation and amplitude restoration in the block mode should be possible.

REFERENCES

1. A. D. Ellis, D. A. O. Davies, A. Kelly, and W. A. Pender, "Data driven operation of semiconductor amplifier loop mirror at 40Gbit/s," *Electron. Lett.*, **vol. 31**, no. 15, pp. 1245-1247, 1995.

2. A. J. Poustie, K. J. Blow, A. E. Kelly, and R. J. Manning, "All-optical full adder with bit-differential delay," *Opt. Comm.*, **vol. 168**, pp. 89-93, 1999.

3. A. J. Poustie, K. J. Blow, A. E. Kelly, and R. J. Manning, "All-optical parity checker with bit-differential delay," *Opt. Comm.*, **vol. 162**, pp. 37-43, 1999.

4. A. J. Poustie, A. E. Kelly, R. J. Manning, and K. J. Blow, "All-optical regenerative memory with full write/read capability," *Opt. Comm.*, **vol. 154**, pp. 277-281, 1998.

5. A. J. Poustie, K. J. Blow, and R. J. Manning, "Storage threshold and amplitude restoration in an all-optical regenerative memory," *Opt. Comm.*, **vol. 146**, pp. 262-267, 1998.

6. K. J. Blow, R. J. Manning, and A. J. Poustie, "Nonlinear optical loop mirrors with feedback and a slow nonlinearity," *Opt. Comm.*, **vol. 134**, pp. 43-48, 1997.

7. R. J. Manning, A. E. Kelly, K. J. Blow, A. J. Poustie, and D. Nesset, "Semiconductor optical amplifier based nonlinear optical loop mirror with feedback: two modes of operation at high switching rates," *Opt. Comm.*, **vol. 157**, pp. 45-51, 1998.

8. J. P. Sokoloff, P. R. Prucnal, I. Glesk, and M. Kane, "A Terahertz Optical Aymmetric Demultiplexer (TOAD)," *IEEE Photon. Tech. Lett.*, **vol. 5**, no. 7, pp. 787-790, 1993.

9. M. Eiselt, W. Pieper, and H. G. Weber, "SLALOM: Semiconductor Laser Amplifier in a Loop Mirror," *IEEE J. Lightwave Tech.*, **vol. 13**, no. 10, pp. 2099-2112, 1995.

10. N. A. Whitaker Jr., M. C. Gabriel, H. Avramopoulos, and A. Huang, "All-optical all-fiber circulating shift register with an inverter," *Opt. Lett.*, **vol. 16**, no. 24, pp. 1999-2001, 1991.

11. R. J. Manning and D. A. O. Davies, "Three-wavelength device for all-optical signal processing," *Opt. Lett.*, **vol. 19**, no. 12, pp. 889-891, 1994.

12. A. E. Kelly, R. J. Manning, A. J. Poustie, and K. J. Blow, "All-optical clock division at 10 and 20GHz in a semiconductor optical amplifier based nonlinear loop mirror," *Electron. Lett.*, **vol. 34**, no. 13, pp. 1337-1339, 1998.